Drips to Drops — Bridging the Gap

Part III Essay
May 2002

Robert James Whittaker
Pembroke College

Abstract

The motion leading up to, and some time after, the detachment of a drop from a dripping tap is relatively easy to describe. However, at the instant of detachment the topology of the fluid shape changes, which gives rise to both a mathematical singularity and a computational difficulty. The form of the flows immediately before and after the instant of separation is examined, with a particular interest in how these are matched through the bifurcation.

 `http://robert.mathmos.net/`

Contents

1 Introduction

1.1 What is Pinch-off?

Given a drop of one fluid surrounded by another, surface tension will tend to drive the interface towards the shape which has the smallest surface area for a given volume; namely that of a sphere. However, if the drop starts off in a far-from-spherical configuration, the inertial and viscous resistance associated with mass fluid transport may mean that the dynamics favour the formation of several smaller spheres. In other words, a surface tension driven instability may cause the fluid to break up into smaller droplets.

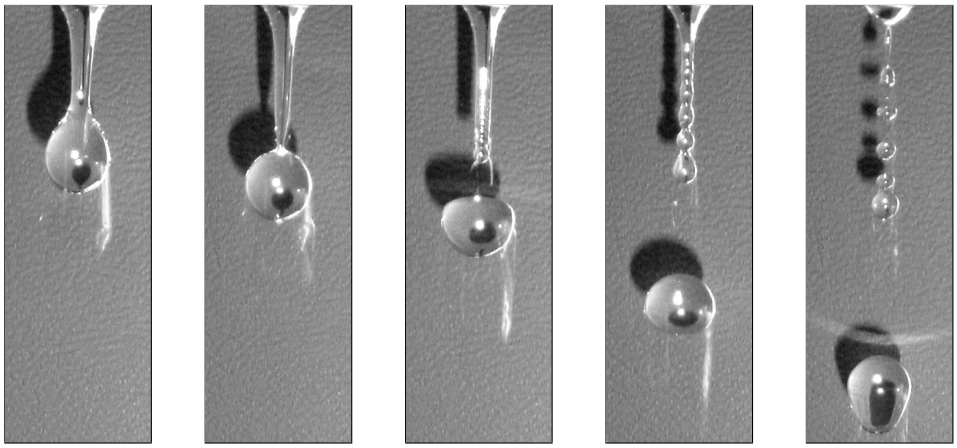

Figure 1: *A sequence of photographs taken by the author using a personal digital camera. It provides an overview of the process of necking, pinch-off, and recoil for water dripping from a tap into air. The width of each image is 14mm, and the total elapsed time for the sequence is of the order of 0.03s.*

Indeed, such fission is a common phenomenon in every-day life. We have all observed a dripping tap, and seen the many small droplets produced by a large stone being thrown into a river. Despite this, the important moments surrounding pinch-off are typically outside our natural visual resolution. Figure 1 shows some of the features that are normally hidden from the naked eye. However, this is still very much a macroscopic view of the pinching process.

The first thing to notice is the distinct lack of up–down symmetry about the minimum radius. This is typical of most pinch-off processes, with a slender filament breaking off from a more bulbous region of fluid. At the

moment of separation, an impulse is given to the tips of the two fluid regions. This causes oscillations of the large drop and sends capillary waves back up the thin filament. In this case, these waves induce secondary bifurcations along the neck, leading to the formation of several so-called satellite drops. Larger photographs, and a more detailed description of a typical bifurcation are given by Peregrine, Shoker, and Symon [16].

1.2 Historical Background

Whilst the fact that liquid filaments tend to fragment was known much earlier, it was not until the latter half of the 19th century that Plateau [17] attributed this breakup to surface tension. Soon after, Lord Rayleigh completed the linear stability analysis for infinite cylinders of both inviscid [19] and highly viscous [20] fluids *in vacuo*.

It is a simple calculation to show that components of an infinitesimal axisymmetric perturbation cause the surface area to increase or decrease as the axial wavelength, λ, is less than or greater then the initial circumference, $2\pi a$. Thus a cylinder is expected to be unstable to precisely those components which satisfy $\lambda > 2\pi a$.

Rayleigh's detailed calculations show that in the Stokes regime, 'infinite' wavelengths grow fastest [20]. However, for a perfectly inviscid fluid, inertia inhibits the growth of long-wave modes, and the dominant wavelength occurs at $\lambda \approx 9a$ [19]. In the 1930s, G.I. Taylor [22] and Tomotika [25], made experimental and theoretical contributions to the problem, including the effects of an outer fluid. Even in the absence of inertia, viscous shearing in the outer fluid limits the grow of long wavelength modes, and the maximum linear growth rate is achieved at a finite wavelength.

In most cases, the fastest-growing linear mode on an infinite cylinder has a finite wavelength. It is this mode which will dominate if the cylinder is subjected to a general perturbation. It is reasonable to assume that similar instability mechanisms will be present in finite elongated drops, and that such instabilities will continue into the non-linear regime. Growing undulations will cause significant deformations, and it is not hard to imagine this process continuing until the original drop breaks apart at one or more points.

Linear theory performs well for small disturbances, and over the years various non-linear corrections have been added to extend its validity. How-

ever, this essay is concerned with the situation far away from the linear regime, when the thinest regions are close to rupture. I shall examine the current research into the form which flows take immediately before and after rupture, and in particular the attempts which have been made to 'bridge the gap' between the two.

1.3 Current Interest

There has recently been much interest in this area, which is of theoretical, numerical, and practical importance. There is a general theoretical interest in the nature of singularities in non-linear systems. This case is particularly interesting since it also involves a change in the topology of the interface and therefore the solution domains.

From a numerical point of view, simulating the flow in the neighbourhood of a singularity is expensive. High velocities, together with short length and time scales mean that small time steps and dense grid points are required. There is the hope of providing a way to 'bridge the gap' and bypass this computational difficulty. In essence a forming singularity would be detected, and then a separate algorithm would be used to calculate the flow around the pinching point at next time step.

Practical applications stem from the realisation that the dynamics of pinch-off affect the recoil of the fluid necks, and are thus a key factor in the formation of smaller satellite drops. This is important to the ink-jet printing industry, and also to those concerned with fluid mixing processes.

2 Preliminaries

2.1 Axisymmetry

A major simplification comes from the assumption that the breakup remains axisymmetric at all times. Not only is this an obvious simple case to study, but it also has theoretical justification. The breakup under consideration is a surface tension driven phenomenon, and the cross-sectional shape which minimises the perimeter (for a given area) is a circle. Thus we would expect that with axisymmetric far field conditions, the flow will be stable to non-axisymmetric perturbations, and will therefore remain axisymmetric.

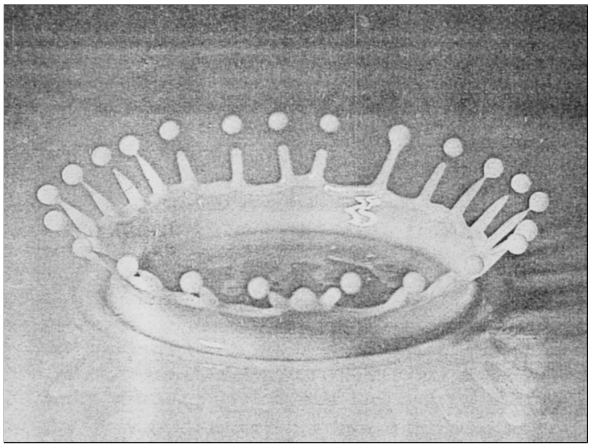

Figure 2: *A Harold Edgerton photograph [7] of the splash due to a milk drop hitting a thin layer of milk on a rigid surface. The sheet-like splash forms cylindrical filaments before pinching to produce drops.*

Even with non-axisymmetric initial conditions, it is perhaps reasonable to assume that, under the action of surface tension, filament-like fluid elements will become axisymmetric as they approach breakup. As shown in figure 2, even liquid sheets may split into several cylindrical filaments before pinching in an axisymmetric fashion.

For these reasons, the literature deals almost exclusively with the case of axisymmetric pinch-off,[1] and in this essay I shall follow suit. Unless otherwise stated, all flows should be taken to be axisymmetric.

[1]The notable exceptions are work by Keller and Miksis [11], and Ting and Keller [23]. They also look at the slightly different problem of liquid sheets in contact with a plane surface, and use planar, rather than an azimuthal, symmetry.

2.2 Separation of Scales and Self-Similarity

A key idea throughout this area of research is that of a separation of scales. As the minimum radius decreases towards zero, the length and time scales of the flow tend to zero, and so become much smaller than any fixed scales. Thus it is reasonable to assume that close to pinch-off, the flow will depend only on the internal fluid parameters, and will be insensitive to initial and far-field conditions. Then there is essentially no difference between the pinch-off at a dripping faucet and in a fragmenting liquid jet.

With a lack of relevant length and time scales, it is natural to seek a similarity solution for the flow just before and just after pinch-off. Little is understood about the mechanisms of rupture on the molecular level, by which point the continuum hypothesis will certainly be invalid. However, it is hoped that such scales will be widely separated from the scales associated with the similarity solutions, so that molecular rupture will be unable to affect significantly the surrounding flow.

Furthermore, it might be hoped that there is some degree of universality in the similarity solutions for the flow before rupture, and that they will be attractors for all pinching flows. The limiting values of such solutions would then be able to provide initial conditions for a solution after pinch-off. As we shall see later, this is often found to be the case.

2.3 Pinching Mechanisms and Force Balance

From an initial linear instability to the final pinching, the driving force is that of surface tension, which tries to minimise the surface area. Gravity or a large-scale straining motion in the outer fluid may well be responsible for drawing a drop of fluid out into a thin thread, which in turn initiates the instability.[2] However, such 'smooth' forces are negligible close to pinch-off, where the diminishing scales allow capillary, viscous, and inertial forces to diverge. For a pinching filament *in vacuo*, a very crude scaling analysis gives estimates for their respective contributions to the momentum equation:

$$F_\gamma \sim \frac{\gamma}{L^2}\,, \quad F_\mu \sim \frac{\mu}{LT}\,, \quad F_\rho \sim \frac{\rho L}{T^2}\,, \tag{1}$$

[2]Recall that surface tension alone stabilises small perturbation with a wavelength less than the circumference on a perfect cylinder. One would expect that, for a finite drop, a reasonable aspect ratio would be required before analogous instabilities can arise.

where γ is the surface tension, μ is the viscosity, ρ is the density, and L and T are suitable length and time scales associated with the shrinking neck.

It is then necessary to decide which of these terms contribute to the leading order force balance close to pinch-off. Clearly, we want to include surface tension since this is driving the flow to rupture. Three different regimes arise when we choose to include either or both of the other two effects. There are also other regimes, which come from considering the effects of an external fluid. Depending on the fluid properties and the far-field conditions, the dynamics may pass through one or more of these regimes before pinch-off finally occurs [13]. The sections which follow look in detail at the progress which has been made in three different regimes.

2.4 Techniques of Analysis

Three different techniques have been used in the literature to examine the fluid flows close close to pinch-off: experiments, numerical simulations, and similarity solutions.

Experiments basically speak for themselves, but the short length scales and time scales involved have inspired clever optical and timing techniques to aid visualisation close to pinch-off.[3]

We are still not sufficiently advanced to perform efficient and accurate simulations of the full Navier–Stokes equations, especially in the neighbourhood of a singularity. However, various simplifications naturally arise which enable simulations to be used to great effect. Neglecting either inertia or viscosity allows boundary integral techniques to be used, and in another case a long-wavelength model is appropriate. When combined with axisymmetry, these allow the discretisation to be reduced from three dimensions to just one.

As mentioned above, the similarity solutions essentially result from a separation of scales. Substituting a suitable ansatz into the governing equations often results in a simpler system. In some cases the similarity equations have themselves been solved numerically. In others a similarity solution has been inferred from the rescaled results of numerical simulations.

[3]Discussion of these experimental techniques is beyond the scope of this essay, but a good starting point for the interested reader would be the work of Kowalewski *et al.* [12], or section II in Eggers' review paper [10].

3 The Inviscid Regime

3.1 Scaling Arguments

In this section, we consider the case of pinch-off that is driven by surface tension, resisted by inertia, and has negligible viscosity. The effects of any surrounding fluid are also ignored. The validity of these last two assumptions is discussed later. A simple order of magnitude balance gives,

$$\gamma \frac{\partial(h^{-1})}{\partial z} \sim \rho \frac{\partial v}{\partial t} \quad \Rightarrow \quad \frac{\gamma}{hz} \sim \frac{\rho z}{\tau^2}\,, \tag{2}$$

where τ is the time to pinch-off, z is the axial coordinate, and h is the radius of the fluid filament. The surface tension is γ, and the fluid density is ρ. The pinching point is set at $z = 0$, and $v \sim z/\tau$ is used as the scale for the axial velocity.[4]

This alone does not give enough information to obtain scales for z, h, and v. However, for irrotational flow, solutions to the Euler Equations are given by $\mathbf{u} = \boldsymbol{\nabla}\phi$, where $\nabla^2\phi = 0$. In the absence of any external preferences, the Laplacian operator will impose $h \sim z$. Adding this to the previous balance, we obtain the following scalings:

$$h \sim z \sim \left(\frac{\gamma\tau^2}{\rho}\right)^{1/3}, \quad v \sim \left(\frac{\gamma}{\rho\tau}\right)^{1/3}. \tag{3}$$

Note that these scalings would also arise solely on dimensional grounds. Since $h \sim z \propto \tau^{2/3}$, this predicts a shrinking pinching region with a roughly constant aspect ratio.

Under these scalings the Reynolds number is estimated as,

$$Re := \frac{\rho U L}{\mu} \sim \frac{\rho v z}{\mu} \sim \left(\frac{\rho\gamma^2\tau}{\mu^3}\right)^{1/3}. \tag{4}$$

Thus for non-zero viscosity, $Re \to 0$ as $\tau \to 0$, and the neglection of viscous effects must be invalid for times sufficiently close to pinch-off. However, all is not lost, since rupture on the molecular scale may occur before viscosity becomes important. From the above, we can see that viscosity would become comparable with inertia when $h \sim \ell_\mu := \mu^2/(\gamma\rho)$.

[4] As as being an obvious choice, this estimate can be obtained using the kinematic boundary condition on the interface. The radial velocity will be expected to scale as $u \sim \dot{h} \sim h/\tau$, and global mass continuity gives $uz \sim vh$. Eliminating u, we obtain the proposed scale.

For water pinching in air at room temperature and pressure, $\ell_\mu \approx 14\,\mathrm{nm}$, which spans only a few molecules. Thus it is likely that an inviscid theory would be appropriate for what is perhaps the most commonly observed case of pinch-off.

3.2 Boundary Integral Simulations

Day, Hinch, and Lister [6] give details of a numerical method based upon a boundary integral technique. The standard velocity potential, $\phi(\mathbf{x}, t)$, is used to describe the flow. The dynamic boundary condition is given by the unsteady Bernoulli equation,

$$\frac{\partial \phi}{\partial t} + \frac{1}{2}\,|\boldsymbol{\nabla}\phi|^2 + \frac{\gamma\kappa}{\rho} = 0\,, \tag{5}$$

which is to be satisfied on the surface $S(t)$. We now introduce the free space Green's function,

$$G\left(\mathbf{x};\mathbf{x_0}\right) := -\frac{1}{4\pi\,|\mathbf{x}-\mathbf{x_0}|}\,. \tag{6}$$

By applying Green's second formula to ϕ and G (with the volume being the interior of the pinching drop), the following relation is obtained, which is valid for $\mathbf{x}_0 \in S(t)$.

$$\int_S G\,\frac{\partial \phi}{\partial n}\,dS = \int_S \phi\,\frac{\partial G}{\partial n}\,dS - \frac{1}{2}\,\phi(\mathbf{x}_0) \tag{7}$$

Given ϕ on a set of nodes on the surface S, equation (7) can be solved for $\partial\phi/\partial n$ at those nodes. Differentiating along the surface gives the tangential velocity $\partial\phi/\partial\mathbf{s}$. Applying the kinematic boundary condition, the fluid velocity on the surface describes how the surface itself evolves in time. Finally, equation (5) allows the calculation of $\partial\phi/\partial t$, which determines how ϕ evolves in time.

By virtue of axisymmetry, the azimuthal integrals can be performed analytically, and we are left only having to perform a one-dimensional discretisation of the surface S. Adaptive grid and time step methods can be employed to ensure adequate resolution and improve efficiency.

Day *et al.* [6] carried out numerous simulations starting from highly elongated drop shapes resembling dumbbells. With suitable initial conditions, the simulations were found to be able to reproduce pinch-off. A typical example can be seen in figure 3a.

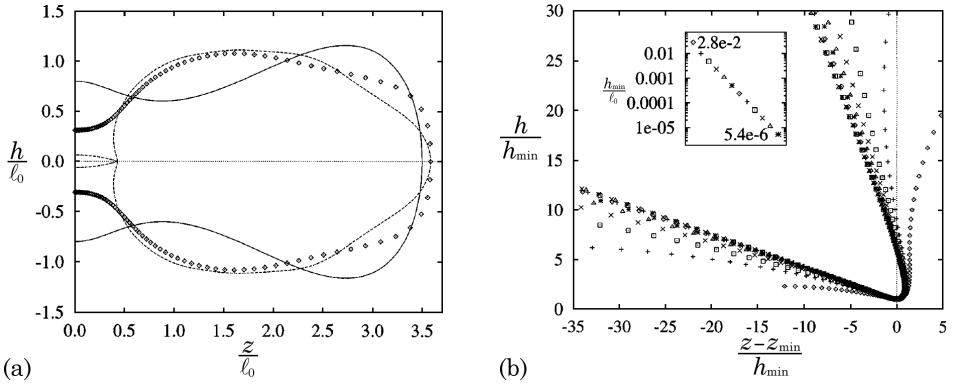

Figure 3: *Two illustrations from Day et al. [6]. The length scale ℓ_0 is associated with the initial drop configuration.* (a) *Three stages in the simulated evolution of a typical drop. Left-right symmetry is imposed for simplicity.* (b) *The detail from the pinching region, with lengths scaled by the minimum radius. The interface is observed to collapse onto a similarity curve.*

Closer investigation of the pinching region confirms the proposed scalings. Both the minimum radius, $h_{\min}$, and the radius at the local axial extremum, h_{nose}, are found to obey $h \propto \tau^{2/3}$, consistent with the radial scaling. Figure 3b was produced by scaling both the radial and axial coordinates by $h_{\min}$, and then plotting how the interface changes over time. This confirms the scalings, and suggests the existence of a similarity solution.

We should also note at this point, the marked asymmetry of the pinch-off. One side consists of a slender conical filament, the other a conical dimple in a much wider volume of fluid. Day *et al.* find that the angles of these cones are independent of the initial conditions. As pinch-off is approached, the limiting angles are always 18.1° and 112.8°. Thus the similarity solution, to which the interface appears to asymptote in figure 3b, may well be universal.

Since the aspect ratio of the pinching region is $O(1)$, and more importantly because of the obtuse angle on one side, the flow is strictly two-dimensional and cannot be modelled by one-dimensional slender jet equations. This may well explain a lack of success in earlier work which made use of such approximations. In particular, it probably accounts for the curvature singularities[5] appearing in the simulations of Brenner *et al.* [2].

[5]Part of the interface was observed to become normal to the axis before pinch-off could occur. This resulted in a singularity within their one dimensional model.

3.3 Similarity Solution and Far Field Conditions

From the evidence of their simulations, Day *et al.* [6] propose the following similarity solution:

$$\phi(\mathbf{x},t) = \Phi(\mathbf{X}) \left(\frac{\gamma^2\tau}{\rho^2}\right)^{1/3}, \quad \mathbf{X} = \mathbf{x}\left(\frac{\rho}{\gamma\tau^2}\right)^{1/3}. \tag{8}$$

Substituting this form into the kinematic and dynamic boundary conditions yields the following pair of equations:

$$\left(\frac{2}{3}\mathbf{X} + \boldsymbol{\nabla}\Phi\right) \cdot \boldsymbol{\nabla}\left(\theta - F(X)\right) = 0 \tag{9}$$

$$\frac{2}{3}\mathbf{X}\cdot\boldsymbol{\nabla}\Phi - \frac{1}{3}\Phi + \frac{1}{2}\left|\boldsymbol{\nabla}\Phi\right|^2 + K = 0\,. \tag{10}$$

Using spherical polar co-ordinates, these are to be satisfied on the appropriately rescaled interface $\theta = F(X)$, whose rescaled curvature is given by K. The scaled potential $\Phi(\mathbf{X})$ must still satisfy Laplace's equation in the interior of the drop.

The far-field conditions are $F \to \alpha$, and $\Phi \sim AX^{1/2}$, which can be inferred from the numerical simulations. Here α (the cone angle) and A are constants, which may well take different values on the two sides. The values of these coefficients inferred from the simulations of Day *et al.* are:

α_+	α_-	A_+	A_-
112.8°	18.1°	2.17	-3.12

Alternatively, the far-field conditions may be derived from the fact that the time dependence must vanish from the laboratory variables as $X \to \infty$ in order to allow the similarity solution to be matched onto a 'slowly varying' outer solution.[6] However, this does not give the *values* of $\alpha_\pm$ and $A_\pm$.

By solving equations (9) and (10) at successive orders (using $\nabla^2\Phi = 0$ to imply the θ dependence), Day *et al.* derive the following series expansions:

$$F(X) = \alpha + \sum_{n=1}^{\infty} F_n X^{-3n/2}\,, \tag{11}$$

$$\Phi(X,\theta) = AX^{1/2}P_{1/2}(\cos\theta) + X^{1/2}\sum_{n=1}^{\infty}\Phi_n X^{-3n/2}P_{3(n-1)/2}(\cos\theta)\,, \tag{12}$$

[6] A similar principle is used by Eggers [9] to derive far-field conditions. It is explained in greater detail, though from a slightly different point of view, in section 4.3.

where $P_s(z)$ denotes the Legendre function of order s. The coefficients F_n and Φ_n are determined from the equations by the two parameters α and A.

In principle, it should be possible to compute the coefficients for each side of the pinching region, and then use fact that the two far fields must be matched through the pinch to determine the four parameters $\alpha_\pm$ and $A_\pm$. However, Day *et al.* report that their attempts to accomplish this were unsuccessful. They are not too concerned though, since the parameters and the similarity shape of the interface (see figure 3b) are already known from their numerical simulations.

3.4 Post-Pinching Planar Flow

The most relevant work on inviscid post-pinching flows is by Keller and Miksis [11], who examine a variety of related flows in a planar geometry. They consider the motion under surface tension of an initially quiescent wedge-shaped volume of fluid in contact with a plane (see figure 4). They find similarity solutions for a range of contact angles, β, and initial wedge angles, α.

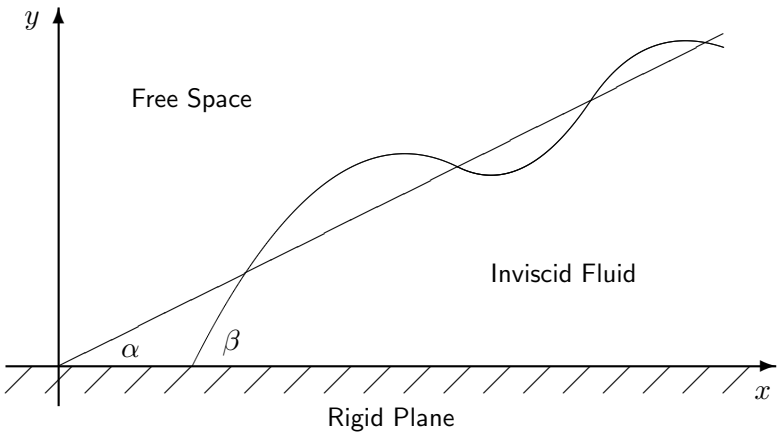

Figure 4: *A diagram of the setup studied by Keller and Miksis [11]. At $t = 0$, stationary inviscid fluid is in contact with a rigid plane, and occupies a wedge of angle α. For $t > 0$, a constant contact angle of β is assumed.*

Since the flow is inviscid, and therefore not subject to a no-slip boundary condition on the plane, the case $\beta = \pi/2$ corresponds to the flow after a line-like pinch-off in a sheet of fluid. Whilst this is not the axisymmetric case with which we are primarily concerned, the methods and results of Keller

and Miksis are highly relevant.

As before, the fluid motion is described by a velocity potential, $\phi(x, y, t)$, and the surface is given by $f(x, y, t) = 0$. The governing equations are Laplace's equation in the fluid,

$$\nabla^2 \phi = 0 \,, \tag{13}$$

together with the dynamic and kinematic boundary conditions on $f = 0$,

$$\frac{\partial f}{\partial t} + \boldsymbol{\nabla}\phi \cdot \boldsymbol{\nabla} f = 0 \,, \tag{14}$$

$$\frac{\partial \phi}{\partial t} + \frac{1}{2} \left| \boldsymbol{\nabla}\phi \right|^2 + \frac{\gamma \kappa}{\rho} = 0 \,. \tag{15}$$

The 'no normal flow' boundary condition on $y = 0$ is applied by removing the boundary and extending the flow domain symmetrically in $y < 0$.

Motivated by dimensional analysis, Keller and Miksis seek a similarity solution with the same scalings as above. Similarity variables are introduced,

$$\xi = x \left(\frac{\rho}{\gamma t^2} \right)^{1/3} , \quad \eta = y \left(\frac{\rho}{\gamma t^2} \right)^{1/3} , \tag{16}$$

and the potential and free surface functions are rewritten as,

$$\phi(x, y, t) = \Phi(\xi, \eta) \left(\frac{\gamma^2 t}{\rho^2} \right)^{1/3} , \quad f(x, y, t) = F(\xi, \eta) \left(\frac{\rho}{\gamma t^2} \right)^{1/3} . \tag{17}$$

The problem of solving Laplace's equation in the fluid is tackled by introducing boundary integrals in an analogous way to that described above. The only difference is that now the two-dimensional form of the Green's function is used:

$$G(\xi, \eta; \xi_0, \eta_0) := \frac{1}{2\pi} \log \left[(\xi - \xi_0)^2 + (\eta - \eta_0)^2 \right]^{1/2} . \tag{18}$$

The similarity functions are then substituted in to the integral equations. After some algebraic manipulations, the system is discretised using N mesh points $\eta = \eta_i$, given by,

$$\eta_i := \frac{i - 1}{N - 1} \, T \quad \text{for } i = 1, 2, \ldots, N \,. \tag{19}$$

The surface is parameterised by $\xi = \Gamma(\eta)$ where possible,[7] and Γ and Φ are discretised as:

$$\Gamma_i := \Gamma(\eta_i)\,, \quad \Phi_i := \Phi(\Gamma_i,\, \eta_i) \tag{20}$$

This yields $2N-4$ equations. The desired far-field and initial conditions are set by,

$$\Gamma_N = T\cot\alpha\,, \quad \text{and} \quad \Phi_N = 0\,, \tag{21}$$

and the contact angle is prescribed by,

$$\Gamma'(0) = \cot\beta\,. \tag{22}$$

Finally, applying the kinematic boundary condition at the tip gives,

$$\left.\frac{\partial\Phi}{\partial s}\right|_{(\Gamma_1,\,0)} = \frac{2}{3}\Gamma_1\cos\beta\,. \tag{23}$$

The derivatives in the last two conditions are approximated using a one-sided Lagrangian difference formula. These four boundary conditions together with the $2N-4$ equations from earlier, are precisely what is required to solve for the $2N$ values $\{\Gamma_i,\, \Phi_i\}$. Keller and Miksis [11] solve this system using Newton's method for various values of α, β, N, and T.

As stated before, the results which are relevant here are those with $\beta = \pi/2$. A selection of such solutions is shown in figure 5.

3.5 Post-Pinching Axisymmetric Flow

Although the calculations have yet to be attempted, it should be possible to follow an analogous route to Keller and Miksis [11] to compute the relevant axisymmetric post-pinching flow. The work of Day, Hinch, and Lister [6] suggests a universal localised pre-pinching similarity solution, with diminishing length scales proportional to $(\gamma\tau^2/\rho)^{1/3}$. As $\tau \to 0$, the pinching region becomes vanishingly small, leaving behind its conical far-field. Assuming that the details of the fission on the molecular scale have negligible effect on this far-field, it makes sense to consider a Keller and Miksis type setup as a suitable model for post-pinching flow.

[7] This is found to work only for α close to $\pi/2$. For smaller α, a conformal transformation can be employed to map the initial wedge onto the whole of the first quadrant: $\xi+i\eta = (\hat{\xi}+i\hat{\eta})^{2\alpha/\pi}$. This transformation introduces a stretching of the coordinates. Keller and Miksis compensate for this by rescaling $\hat{\eta}$ to obtain a more satisfactory distribution of mesh points.

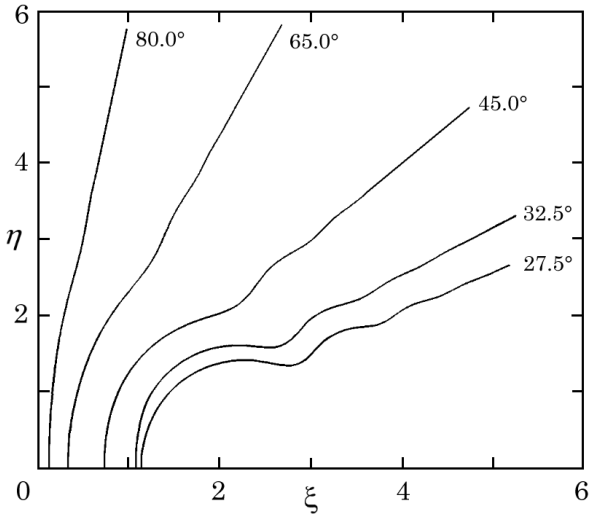

Figure 5: *Interfacial similarity solutions calculated numerically by Keller and Miksis [11]. They represent post-pinching solutions in a planar geometry, and have the initial condition of a wedge of fluid with zero velocity.*

However, two significant changes are required. First it is necessary to switch from a planar to an axisymmetric geometry. The relevant cone angles $\alpha_\pm$ are determined by the pre-pinching solutions. The full three-dimensional Green's function (equation 6) is now needed, which will lead to a stronger $1/r$ singularity in the surface integrals.

Secondly, the initial flow is no longer zero. From section 3.3, we have an initial condition of form,

$$\phi(\mathbf{x}, 0) = A_\pm \left(\frac{\gamma}{\rho}\right)^{1/2} x^{1/2} P_{1/2}(\cos\theta)\,, \tag{24}$$

where the coefficients $A_\pm$ are again determined by the pre-pinching solutions. Due to finite wave speeds, this also becomes a far-field condition as the post-pinching solution evolves.

Finally, there are some technical questions about how the solution will be carried out. Will it be possible to use the Keller and Miksis boundary integral technique, or could the solution be obtained using an expansion similar to that proposed by Day *et al.* for the pre-pinching flow? In the Keller and Miksis method, is it better to employ their conformal transformation of the similarity variables, or use the more natural spherical polar co-ordinates?

4 The Navier–Stokes Regime

4.1 Scaling Arguments

In this regime we consider the pinching of a single fluid with viscous, capillary, and inertial forces all being present in the leading order force balance. A simple scaling argument [13] balancing these three terms in the Navier–Stokes equations gives:

$$\gamma\frac{\partial(h^{-1})}{\partial z} \sim \rho\frac{\partial v}{\partial t} \sim \mu\frac{\partial^2 v}{\partial z^2} \quad \Rightarrow \quad \frac{\gamma}{hz} \sim \frac{\rho z}{\tau^2} \sim \frac{\mu}{\tau z}\,, \tag{25}$$

where τ is the time to pinch-off, z is the axial coordinate, and h is the radius of the fluid filament. The pinching point is set at $z = 0$, and the axial velocity is estimated as $v \sim z/\tau$. These relationships then yield the following scalings:

$$z \sim \ell_\mu \left(\frac{\tau}{t_\mu}\right)^{1/2}, \quad h \sim \ell_\mu \left(\frac{\tau}{t_\mu}\right), \quad v \sim \frac{\ell_\mu}{t_\mu}\left(\frac{\tau}{t_\mu}\right)^{-1/2}, \tag{26}$$

where $\ell_\mu := \mu^2/(\gamma\rho)$ and $t_\mu := \mu^3/(\gamma^2\rho)$ are the natural length and time scales based upon the internal fluid parameters.[8] Thus as $\tau \to 0$ the radial scale vanishes faster than the axial scale, which would indicate that a long wavelength extensional flow approximation may be appropriate.

Under these scalings the Reynolds number is necessarily of order one. Unlike the regimes which result from neglecting either inertia or viscosity, the balance remains consistent as pinch-off is approached. Unless molecular scales (causing rupture) are reached first, the Navier–Stokes balance will always be the final regime for single fluid pinch-off.

4.2 Similarity Equations

In the main paper on the subject,[9] Eggers [9] proceeds by formally expanding the terms in the Navier–Stokes equations in a radial parameter. Two assumptions are used to find the equations governing the leading order quantities.

[8] Clearly other length and time scales are possible if we were to include gravity or an external strain rate. However, as argued in section 2.3, these are irrelevant close to pinch-off and so should not appear in the analysis.

[9] There is short letter [8] (also by Eggers), which gives a brief account of the earlier work in [9]. Papageorgiou [14] has also contributed, using different techniques to derive the same pre-pinching similarity equations and boundary conditions given below.

1. The singularity is line-like, i.e. the axial scale is much greater than radial scale.

2. Surface tension, viscous, and inertial forces are equally important near the singularity.

Since τ is the only external time scale, and in the absence of a suitable external length scale, a similarity solution is proposed. The scalings found above by more *ad hoc* means are recovered with the similarity representation,

$$h = \ell_\mu \, H(\xi) \left(\frac{\tau}{t_\mu}\right), \quad v = \frac{\gamma}{\mu} V(\xi) \left(\frac{\tau}{t_\mu}\right)^{-1/2}, \quad \xi = \frac{z}{\ell_\mu}\left(\frac{\tau}{t_\mu}\right)^{-1/2}. \quad (27)$$

The similarity ansatz is then substituted into a long-wavelength extensional flow approximation to the Navier–Stokes equations. This comprises the leading order terms in the expansion mentioned above. The system is reduced to a coupled pair of ordinary differential equations (axial momentum balance, and the kinematic boundary condition) in the single variable ξ.

$$\left(\frac{V+\xi V'}{2}\right) + VV' = \frac{H'}{H^2} + 3V'' + \frac{6V'H'}{H}, \quad (28)$$

$$\left(-H + \frac{\xi H'}{2}\right) + VH' = -\frac{V'H}{2}. \quad (29)$$

The aim now is to solve this third-order system numerically. In order to do this, suitable boundary conditions need to be formulated.

4.3 Boundary Conditions

Eggers [9] argues that 'sufficiently far' from the pinching point, the fluid flow will not be able to follow the forming singularity. Specifically, he considers a point $z = \ell_\mu \delta$, where $\delta \ll \min\{1, L/\ell_\mu\}$, and L is a characteristic external length scale. Then at small τ, the point $z = \ell_\mu\delta$ will be well inside the range of validity of the similarity solution. However, this point is fixed in the laboratory frame, and axial length scales tends to zero as we approach the singularity. Thus $h(\ell_\mu\delta, \tau)$ is unable to follow the motion near the pinch point, and must tend to a finite value.

Since $\xi \propto z\tau^{-1/2}$, the point in question tends to infinity in similarity variables as $\tau \to 0$. From the form of the similarity expression for h, it can be seen that $H(\xi)$ must grow quadratically as $\xi \to \pm\infty$. Similarly, $V(\xi)$ must decay like ξ^{-1} at infinity. This argument effectively says that the

time dependence must drop out of h and v as $\xi \to \pm\infty$, allowing the inner similarity solution to be matched onto a 'slowly varying' outer solution.

Eggers goes on to demonstrate that such a pair of conditions at $\xi = +\infty$ corresponds to precisely one boundary condition on the system. By eliminating H between the equations, he is able to derive asymptotic expansions about infinity. It is found that up to exponentially small corrections, solutions to (28) and (29) which extend to infinity form a two-parameter family of functions. Furthermore this class of functions has the required behaviour at infinity. The expected third degree of freedom must either correspond to exponentially small deviations, or a class of solutions which do not extend to infinity. By examining the stability of the functions within the two-parameter family, Eggers establishes that the latter applies. Therefore the set of solutions consistent with the the two conditions at positive infinity is a two-parameter family. This argument applies equally at $\xi = -\infty$.

The restrictions at $\xi = \pm\infty$ therefore give us two boundary conditions on the third order system. The final condition comes from demanding that $H(\xi)$ and $V(\xi)$ are regular for all $\xi \in \mathbb{R}$, and that $H(\xi) > 0$ since it represents the fluid radius. By re-arranging (29), we obtain,

$$H' = H\,\frac{1 - V'/2}{V + \xi/2}\,. \tag{30}$$

Since $V(\xi) \to 0$ as $\xi \to \pm\infty$, there must be a point, ξ_0, which satisfies,

$$V(\xi_0) + \xi_0/2 = 0\,. \tag{31}$$

Then for the regularity condition to be met, we must also have,

$$V'(\xi_0) = 2\,. \tag{32}$$

It is easy to show that ξ_0 is in fact a stagnation point. This is in the sense that the fluid velocity there is equal to velocity with which ξ_0, and therefore the fluid interface, moves in the laboratory frame. For future use, I shall define $H_0 := H(\xi_0)$.

4.4 Numerical Solution of the Equations

Eggers [9] employs a 'shooting' technique to solve the equations, starting from a chosen (ξ_0, H_0) pair and integrating out towards either $\pm\infty$. To begin with, a Taylor expansion is made about ξ_0, and the Taylor coefficients

are shown to be completely determined by the chosen values of ξ_0 and H_0. Then, to get beyond the (finite) radius of convergence, the integration is continued numerically. Generally, these numerical solutions do not extend to infinity, but result in a singularity at finite ξ. This is consistent with the asymptotic analysis outlined in the previous section.

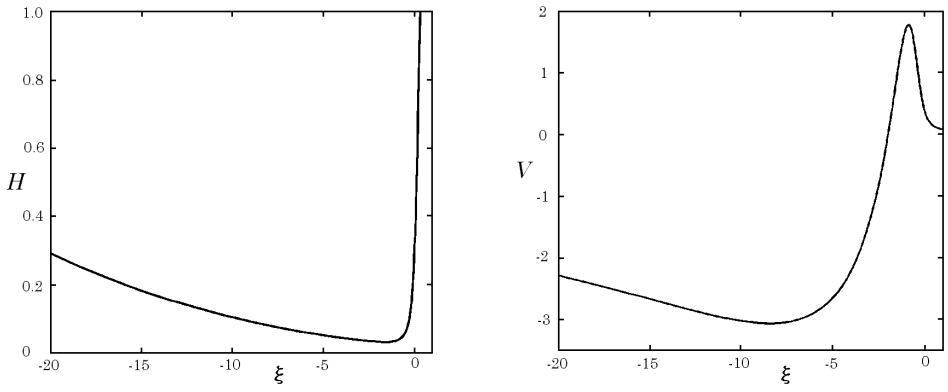

Figure 6: *Plots of similarity functions $H(\xi)$ and $V(\xi)$, which were computed by Eggers [9].*

Eggers finds (as expected) that applying the conditions at either plus or minus infinity restricts the solutions to a one-parameter manifold in (ξ_0, H_0) space. Any points where these two manifolds coincide will correspond to a complete solution of the system. In [9], Eggers reports finding only one such solution.[10] The corresponding similarity functions H and V are shown in figure 6, and their properties are summarised in the following table.

ξ_0	H_0	$\xi_{\min}$	$H_{\min}$	$V_{\max}$
-1.5699	0.030432	-1.6024	0.030426	-3.066

a_+	b_+	a_-	b_-
4.635	0.0723	6.047×10^{-4}	57.043

The numbers $a_\pm$ and $b_\pm$ give the far-field behaviour, and are defined as,

$$a_\pm := \lim_{\xi \to \pm\infty} \xi^{-2} H(\xi)\,, \quad b_\pm := \lim_{\xi \to \pm\infty} \xi\, V(\xi)\,. \tag{33}$$

[10] In this solution, the functions H and V are not symmetric about the origin. The transformation $\xi \mapsto -\xi$ will yield another equally valid solution, but his is not regarded as distinct. Without loss of generality, we may restrict attention to $\xi_0 < 0$.

4.5 Post-Pinching Flow

Even though the equations used by Eggers *et al.* are only approximations to the Navier–Stokes equations, they will become asymptotically exact as $\tau \to 0$. Likewise, while a similarity solution might not represent the exact flow for any $\tau > 0$, it might be hoped that in the limit $\tau \to 0$, the flow may be modelled precisely by the similarity solution. Furthermore, it is hoped that the microscopic details of the actual breakup on the molecular scale will have negligible effect on the bulk of the fluid surrounding the singularity. Then the limiting flow profile (velocity and radius) at $\tau = 0$ can be used as an initial condition for the flow after pinch-off.

Eggers [9] uses the same procedure as described in section 4.2 to derive the following system of similarity equations which govern flow the immediately after breakup has occurred.

$$-\left(\frac{V+\xi V'}{2}\right) + VV' = \frac{H'}{H^2} + 3V'' + \frac{6V'H'}{H}, \tag{34}$$

$$-\left(-H + \frac{\xi H'}{2}\right) + VH' = -\frac{V'H}{2}. \tag{35}$$

This pair of equations can be seen to be almost identical to (28, 29), the only difference being the two minus signs in front of the bracketed terms (which correspond to the time derivatives). The similarity functions and variables are as defined previously, but now τ is the time *after* rupture.

Since these equations are based upon a long-wavelength approximation, they cannot be valid in a region near the tip of the receding necks of fluid. Eggers considers this region separately (by including higher order terms), and derives the following boundary conditions for the bulk similarity flow:[11]

$$H(\xi_{\text{tip}}) = \frac{1}{6}\,, \quad V(\xi_{\text{tip}}) = \frac{\xi_{\text{tip}}}{2}\,. \tag{36}$$

The first condition states that the height of the fluid near the tip is effectively a step function. In other words, the region where the extensional flow equations are not valid is asymptotically small compared to scales of the bulk the similarity flow. The second condition is merely a kinematic

[11] It is interesting to compare this tip approximation to that of Papageorgiou [14], which involves strapping a blob of fluid onto the tip. Both methods follow the same scalings and use the same slender jet equations for the bulk similarity flow. Unfortunately, there is a lack of relevant data to allow a full comparison of the predicted flow profiles.

boundary condition; the velocity of the receding tip must equal the fluid velocity there.

The remaining boundary conditions come from the behaviour of H and V at infinity. Recall from section 4.3, that a fixed point z tends to infinity in similarity variables as the singularity is approached. Thus the matching of the pre-pinching and post-pinching solutions is achieved by demanding the same asymptotic behaviour of H and V at infinity. Specifically, the post-pinching solutions must satisfy:

$$\xi^{-2}\, H_{\pm}(\xi) \to a_{\pm} \quad \text{and} \quad \xi\, V_{\pm}(\xi) \to b_{\pm} \quad \text{as} \quad \xi \to \pm\infty\,, \tag{37}$$

where the '$\pm$' differentiates between the two separate solutions required for the two separate receding necks formed after the bifurcation.

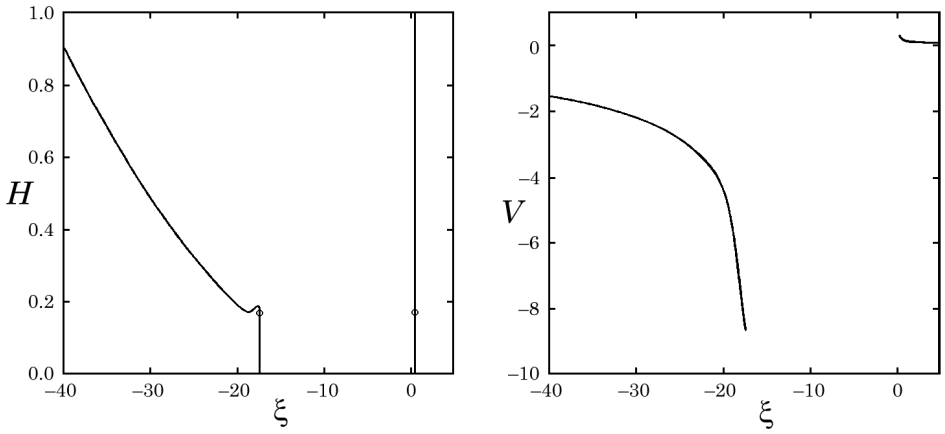

Figure 7: *The post-pinching similarity solutions computed by Eggers [9].*

Eggers uses a series expansion about ξ_{tip}, and shows that given the conditions (36) at the tip, possible solutions belong to a two-parameter family, being labelled by ξ_{tip}, and one other coefficient. These series expansions have only a finite radius of convergence, so further integration towards infinity is completed numerically.

In contrast to the equations governing the flow before breakup, the asymptotic behaviour of $H \sim A\xi^2$ and $V \sim B\xi^{-1}$, is now stable. Integrating the equations to infinity (from an arbitrary ξ_{tip}) yields a pair of values for:

$$\lim_{\xi\to\infty} \xi^{-2}\, H(\xi) \quad \text{and} \quad \lim_{\xi\to\infty} \xi\, V(\xi)\,. \tag{38}$$

Thus the values of $a_\pm$ and $b_\pm$ from the pre-pinching solution are precisely what is required to determine unique solutions for H and V after breakup. Eggers [9] finds the post-pinching similarity solutions for both sides of the ruptured ligament. These represent the continuation of the flow through the singularity, and are shown in figure 7.

4.6 Results of Experiments and Numerical Simulations

The question which arises naturally at this point is whether or not the proposed similarity solutions are realised in experiments and numerical simulations.

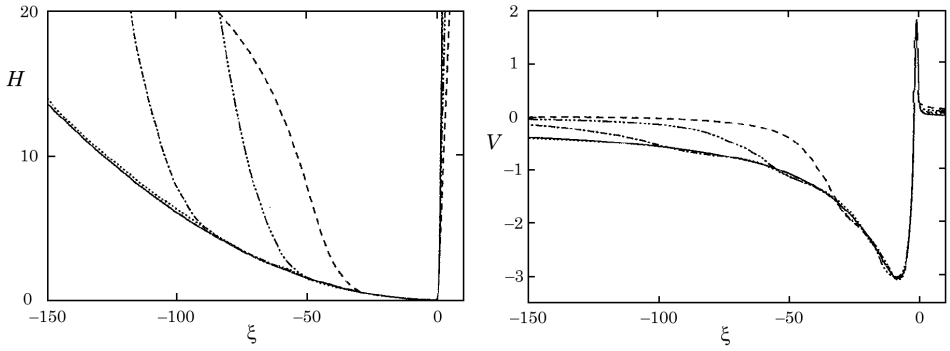

Figure 8: *The solid lines show Eggers' similarity solutions. The dashed, chain-dashed, dot-dashed, and dotted lines show the results of a numerical simulation [9] at* $\tau/t_\mu = 0.39, 0.13, 0.043, 0.014$ *respectively.*

The pre-pinching solution found by Eggers is seen in both experiments and numerical simulations. Eggers' own simulations [9] using the his one-dimensional model of the Navier–Stokes equations show excellent convergence to the both the pre-pinching and post-pinching solutions that he proposed (see figure 8).

However, the similarity solution does not compare as well with experiments. For a while there is very good agreement (see figure 9), but the long neck which is formed tends to undergo secondary instabilities rather than remaining self-similar. It is observed that these instabilities lead to the formation of a secondary neck on a smaller scale. This neck then follows the Eggers similarity solution for a while before developing further instabilities. This process is believed to continue until molecular scales are reached and the thread finally ruptures.

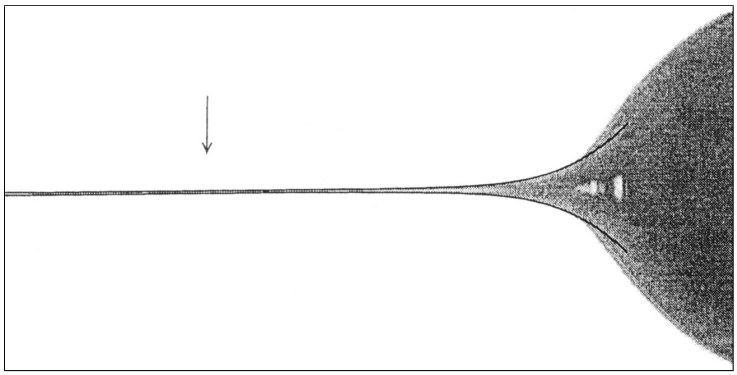

Figure 9: *A Photograph of an experiment by Kowalewski [12], which has been overlaid with the appropriate Eggers similarity solution. The frame width is about 1.5mm, and the time to rupture is 615μs. The arrow marks the minimum radius.*

This cascade of instabilities was first reported by Shi, Brenner, and Nagel [21]. They managed to reproduce qualitatively such instabilities by adding a small amount of noise to their numerical simulations. Without such artificially added noise, the simulations remain stable. Brenner *et al.* [3] liken these instabilities to the Rayleigh instability of cylindrical fluid filament. They show that at an arbitrary $h_{\min}$, the linear growth rate of such instabilities would be large enough for appreciable growth to occur in the time remaining before rupture. Generally, the large velocities in the necking region will convect such instabilities away, but for disturbances near the stagnation point, ξ_0, this will not be the case.

A linear stability analysis of the similarity solution [3] shows that this reasoning is essentially correct. Maximum growth is achieved for perturbations with a wavelength of order $h_{\min}$ which occur near the stagnation point at ξ_0. Moreover, there is a critical amplitude, A_c, which must be exceeded before the perturbations will grow.

$$A_c \approx 10^{-6.2} \ell_\mu \left(\frac{\tau}{t_\mu} \right)^{2.49} \tag{39}$$

The fact that there is a finite cut-off amplitude explains why previous numerical simulations failed to show signs of the instabilities that have been observed in experiments. Since $A_c \to 0$ as pinch-off is approached, it seems inevitable that real experiments will exhibit these instabilities. Even if all other sources of noise could be eliminated, thermal fluctuations would even-

tually be sufficient.

As a result of these instabilities, the singularity at fission is characterised by a rough interface. It is unclear whether this alone accounts for the large discrepancies observed by Kowalewski [12] between his experiments and Eggers' post-pinching solution. It is an open question as to whether an experiment which was sufficiently free from external noise (necessarily at low temperature) would be able to recover Eggers' post-pinching solution. Indeed would such an experiment even be feasible?

4.7 Additional Pre-Pinching Similarity Solutions

Despite Eggers' expectation that his pre-pinching solution would be unique, and its reproduction in both experiments and simulations, further solutions to the system (28, 29) have been found. Brenner, Lister, and Stone [1] examined the power series expansions of H and V around ξ_0. They found that the recurrence relations for the coefficients were singular whenever,

$$H_0 = H_*(n) := \frac{1}{15n - 12}\,, \quad n = 1, 2, 3, \ldots\,. \tag{40}$$

The striking similarity of $H_*(3) = 0.0303\ldots$ and the $H_0 = 0.0304\ldots$ in the solution found by Eggers, lead them to look for new solutions near the other singular points.

Additional solutions were found close to $H_*(n)$ for $n \in \{7, 11, 15, 19, 21\}$, and it is conjectured by Brenner *et al.* that this pattern will continue indefinitely. In other words they propose the existence of an infinite family of solutions to (28, 29), where the Nth solution satisfies the approximate rule:

$$H_{\min}(N) \approx H_0(N) \approx \frac{1}{60N - 27}\,, \quad N = 1, 2, 3, \ldots\,. \tag{41}$$

Brenner *et al.* [1] have calculated the first six solutions explicitly, and while they retain the qualitative character (including the marked asymmetry) of the original Eggers solution, they each exhibit very different values of $a_\pm$ and $b_\pm$ (the far-field coefficients).

Part of the reason Eggers failed to find these new solutions must have been that there was no need for additional flow profiles; the simulations he performed fitted perfectly well with the solution he had found. Interestingly, simulations repeatedly fail to reproduce these new solutions.

Brenner, Lister, and Stone [1] performed a stability analysis on these new solutions, in a similar fashion to that previously carried out by Brenner, Shi,

and Nagel [3]. The critical amplitude for the Nth solution is found to be given by:

$$A_c = C_\sigma \, \ell_\mu \, H_0(N)^\sigma \left(\frac{\tau}{t_\mu}\right)^{1+\sigma/2} , \tag{42}$$

where C_σ is a dimensionless constant, and $\sigma \approx 4N - 1$. Thus A_c diminishes much more rapidly as $\tau \to 0$ with increasing N. C_σ and $H_0(N)$ also decrease with increasing N. It follows that the new solutions are much more prone to instabilities than Eggers' original solution.

Simulations, reported in the same paper [1], show that starting with one of the new solutions as the initial conditions, it destabilises, and then forms a new similarity-type solution. Exactly which of the solutions is realised is found from looking at the value of a_+, which varies significantly between the different solutions. In every simulation, the Eggers solution was formed. This behaviour is rationalised by Brenner *et al.* who argue that following destabilisation, an initially flat region steepens until an allowable asymptotic curvature is reached. These allowable curvatures are given by the values of a_+ corresponding to the similarity solutions. Since the Eggers solution has the lowest value of a_+, it is reached first. Therefore the instabilities lead to the new asymptotic solution being the one derived by Eggers.

5 The Two Fluid Viscous Regime

5.1 Scaling Arguments

To this point we have dealt exclusively with the pinch-off of a single fluid *in vacuo*, or to be more precise, the case where the effects of the outer fluid are assumed to be negligible. It might be thought that this is a reasonable assumption whenever the outer fluid has a very low viscosity and density in comparison with the inner fluid.

However, Lister and Stone [13] showed that things are not quite this simple. Just as it is asymptotically inconsistent to neglect either inertia or viscosity in single fluid pinch-off,[12] it is also inconsistent to neglect the effects of an outer fluid.

For single fluid pinch-off, the final asymptotic balance is the Navier–Stokes regime discussed in section 4. Consider applying the scalings of this regime to the case where a pinching thread of viscosity μ_i is surrounded by an external fluid of viscosity μ_e. The axial flow in the thread will drive a flow in the outer fluid. Let the radial length scale for this flow be δ.

Estimates for the two viscous contributions (internal extension, and external drag) to the axial momentum balance are made as follows. The total resistance is estimated as the product of the appropriate viscosity, velocity gradient, and area of action. This is then divided by the corresponding volume of internal fluid. We find that:

$$\text{Internal Contribution} \sim \frac{\mu_\mathrm{i}\,(v/z)\,h^2}{zh^2} = \mu_\mathrm{i}\frac{v}{z^2} \propto \tau^{-3/2} \tag{43}$$

$$\text{External Contribution} \sim \frac{\mu_\mathrm{e}\,(v/\delta)\,\delta z}{zh^2} = \mu_\mathrm{e}\frac{v}{h^2} \propto \tau^{-5/2} \tag{44}$$

Unless $\mu_\mathrm{e} \equiv 0$, the external drag will eventually dominate as $\tau \to 0$. Thus the Navier–Stokes scalings in section 4.1 must eventually give way to a new balance, unless molecular scales (causing rupture) are reached first. It is easy to see that the transition would occur at $\tau \sim (\mu_\mathrm{e}/\mu_\mathrm{i})\,t_\mu$, while molecular scales are reached when $\tau \sim (\ell_\mathrm{mol}/\ell_\mu)\,t_\mu$. The physical properties of the fluids involved determine which is reached first.

[12] The consequences of neglecting viscosity are dealt with in section 3. The case of neglecting inertia is omitted for the sake of brevity, but a suitable reference is [15].

Lister and Stone [13] propose that the new balance will be dominated by capillary forces, internal extension, and external drag. Using $v \sim z/\tau$ as before, this leads to:

$$\gamma \frac{1}{hz} \sim \mu_{\mathrm{i}} \frac{1}{\tau z} \sim \mu_{\mathrm{e}} \frac{z}{\tau h^2}\,, \tag{45}$$

and thence the scalings:

$$z \sim \frac{\gamma\tau}{\lambda^{1/2}\mu}\,, \quad h \sim \frac{\gamma\tau}{\lambda\mu}\,, \quad v \sim \frac{\gamma}{\lambda^{1/2}\mu}\,, \tag{46}$$

where by convention, we have written $\mu_{\mathrm{e}} = \mu$, and $\mu_{\mathrm{i}} = \lambda\mu$.

Since $z \sim \lambda^{1/2} h$, these scalings predict a constant $O(\lambda^{1/2})$ aspect ratio close to pinch-off. It should also noted that in the above analysis there is the implicit assumption that the external viscosity is comparable to or less than the internal viscosity, i.e. $\lambda \geq O(1)$. This is used in estimating the magnitude of the viscous response in the internal fluid. Hence the analysis *may not* be appropriate for the breakup of a relatively invicid bubble in a viscous fluid.

Under these scalings, the Reynolds number is found to be proportional to τ, which is consistent with the neglection of inertial terms close to pinch-off. Lister and Stone argue that this should be the final regime (unless molecular rupture occurs first) for any pair of fluids with $\lambda \geq O(1)$.

5.2 Stokes Flow Boundary Integral

The scaling analysis above suggests that inertia will be negligible close to pinch-off. Motivated by this, Lister and Stone [13] performed some numerical simulations of the stokes flow driven by the surface tension at a two-fluid interface. They make use of a boundary integral representation, which allows the velocity of the interface to be found without having to compute the details of the flow.

Specifically, if the (closed) interface is given by $S(t)$, then for $\mathbf{x}_0 \in S(t)$, it may be shown [18] that the following relation holds:

$$\frac{1}{2}\,(1+\lambda)\,\mathbf{u}(\mathbf{x}_0) + (1-\lambda)\int_{S(t)} \mathbf{n}\cdot\mathbf{K}\cdot\mathbf{u}\; dS = -\gamma \int_{S(t)} \kappa\,\mathbf{n}\cdot\mathbf{J}\; dS\,, \tag{47}$$

where κ is the surface curvature, dS is the interfacial surface area element, and $\mathbf{n}$ is the outward normal (all evaluated at $\mathbf{x}$). Also,

$$\mathbf{J}(\mathbf{r}) := \frac{1}{8\pi\mu}\left(\frac{\mathbf{I}}{r} + \frac{\mathbf{rr}}{r^3}\right)\,, \quad \mathbf{K}(\mathbf{r}) := -\frac{3}{4\pi}\,\frac{\mathbf{rrr}}{r^5}\,, \quad \mathbf{r} := \mathbf{x}_0 - \mathbf{x}\,. \tag{48}$$

A numerical scheme uses this representation to compute $\mathbf{u}$ at a set of N mesh points on the interface. By virtue of axisymmetry, this can be reduced to a one-dimensional discretisation. For $\lambda = 1$ there is an obvious further simplification. For $\lambda \neq 1$, an integral equation must be solved (which reduces to the inversion of an $N \times N$ matrix) to obtain $\mathbf{u}$.

Once $\mathbf{u}$ is known on the interface, we can compute the position of the interface at the next time step. Adaptive methods are employed so that each time step corresponds to decreasing the minimum radius by at most a certain small fraction. Also, the grid points are redistributed (and possibly N increased) at each step, to ensure an adequate resolution of the interface, especially in regions of high curvature.

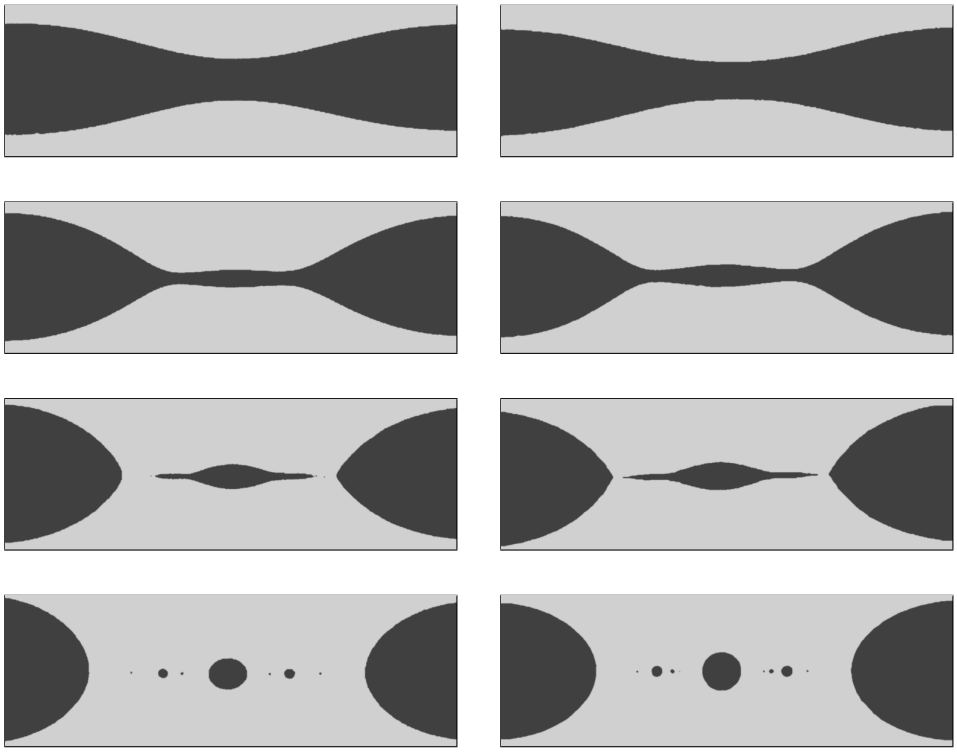

Figure 10: *Experimental (left) and computational (right) results from [24]. The pictures show a filament pinching under surface tension effects. The viscosity ratio is $\lambda = 0.067$, and the width of each image is 5mm.*

The success of this method is evident from related work by Tjahjadi *et al.* [24] who used the boundary integral technique to simulate the formation of satellite drops from a long thin thread (see figure 10). The numerical

results show remarkable agreement with their experiments. This supports not only the accuracy of the boundary integral method, but also the validity of neglecting inertia.

5.3 Simulations for $\lambda = 1$

For the case $\lambda = 1$, Lister and Stone [13] performed numerous simulations using the scheme outlined above. Pinch-off was found to occur for suitable elongated initial drop shapes. Lister and Stone were able to confirm their scaling arguments in all but one respect; the prediction that the axial velocity remains $O(\gamma/\mu)$ is not accurate. I shall come to this later.

Sufficiently close to pinch-off, it was found that minimum radius, $h_{\min}$, did indeed decrease linearly in time. This supports the proposed axial scaling with $h \propto \tau$. To further examine the simulations, both the axial and radial lengths are rescaled by $h_{\min}$. This is more convenient than using τ, which would require the estimation of the exact pinch-off time. The axial velocity is scaled by the fluid parameters. The new dimensionless variables used to plot the results are then,

$$H := \frac{h}{h_{\min}}\,, \quad V := \frac{\mu\, v}{\gamma}\,, \quad \zeta := \frac{z - z_{\min}}{h_{\min}}\,, \tag{49}$$

with $z_{\min}$ being the value of z at the minimum radius.

Lister and Stone plot rescaled profiles of the interface radius (figure 11a), the axial curvature, and the axial strain rate. All of these demonstrate excellent collapse onto similarity curves as $\tau \to 0$. Furthermore, these curves are found to be independent of the initial conditions. In particular, the interface just outside the pinching region takes the form of a pair of cones, with semi-angles given by 5.9° and 78.2°. Once again there is a significant asymmetry in the pinch-off.

Although the strain rate, $\partial v/\partial z$, is found to be self-similar, the axial velocity, v, is not. As can be seen in figure 11b, the scaled velocity, $V(\zeta)$, increases as the the fluid pinches. Further analysis of the data leads to the model,

$$V = -0.0243 \log h_{\min} + \text{const}\,. \tag{50}$$

The constant depends on both the value of ζ at which V is to be evaluated, and the initial conditions (since it varies between different simulations). Obviously, $h_{\min}$ can be replaced by τ and the constant adjusted appropriately.

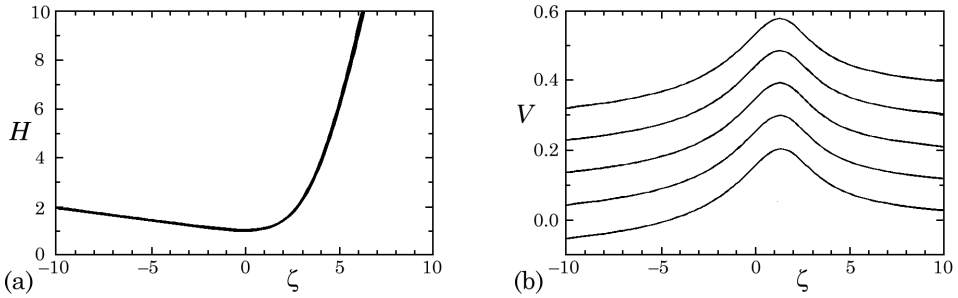

Figure 11: *Rescaled plots from Stokes flow simulations [13].* (a) *The fluid interface collapses onto a similarity curve, independent of the initial conditions.* (b) *The axial velocity shows a steady increase, contrary to the scaling analysis estimate.*

Since the non-similarity component of V is a uniform velocity, its effect is simply to advect the pinching region, without deforming the interface or upsetting the other scalings.

Lister and Stone [13] attribute this logarithmic velocity contribution to non-local effects from the conical region of the interface. Define ℓ_0 as a suitable macroscopic length scale for the pinching drop, and let $\ell_\tau := \gamma\tau/\mu$ be the length scale associated with the pinching region. The pinching drop can then be divided into three regions:

- The inner pinching region; $|z - z_{\min}| = O(\ell_\tau)$.
- An intermediate conical region; $\ell_\tau \ll |z - z_{\min}| \ll \ell_0$.
- The macroscopic far field; $|z - z_{\min}| = O(\ell_0)$.

By virtue of boundary integral formula (47), the velocity can be written as an integral over the surface. Now consider the nature of the contributions to the velocity in the pinching region from the three different regions of the drop. In the far field, we have an $O(\ell_0)$ scale of variation, so any induced velocity in the pinching region will appear to be uniform and constant relative to the small scales within the pinching region. This probably accounts for the variation in the constant between different simulations.

From within the pinching region itself, the induced velocity is $O(\gamma/\mu)$ with a length scale of $O(\ell_\tau)$. A pure similarity solution would be governed solely by this contribution. However, the intermediate conical region contributes stresses which generate a shear rate of $O[\gamma/(\mu z)]$. Thus the con-

tribution to the velocity is $O[(\gamma/\mu)\log(\ell_0/\ell_\tau)]$. The relevant length scale is still $\gg \ell_\tau$ so this velocity appears spatially uniform in the pinching region. Since $h_{\min} \sim \ell_\tau$ this is precisely the contribution required.

Lister and Stone calculate the asymptotic contributions from an intermediate region comprising a pair of perfect cones. They derive an expression relating the log coefficient to the cone angles (equation 56). The numerical values from their simulations are found to be consistent with this expression.

5.4 Similarity Solution for $\lambda = 1$

Motivated by the results of the simulations reported above, Cohen *et al.* [5] propose a similarity solution. Their explanation is a little unclear, and I have made a couple of notational changes which I feel improve matters. The form I would propose is as follows:

$$h(z,t) = \frac{\gamma\tau}{\mu} H(\xi)\,, \tag{51}$$

$$\mathbf{u}(\mathbf{x},t) = \frac{\gamma}{\mu}\Big[U(\xi)\,\hat{\mathbf{r}} + \Big(V(\xi) + b\log\tau + c\Big)\hat{\mathbf{z}}\Big] \quad \text{on } r = h\,, \tag{52}$$

$$\xi = \frac{\mu}{\gamma\tau} z + b\,(\log\tau - 1) + c\,. \tag{53}$$

This is essentially a standard similarity representation (using the previous scalings) to which a background axial velocity ($b\log\tau + c$) has been added. Since this will advect the interface, the location of $\xi = 0$ has been set to translate with this velocity too. The pinching point is fixed at $z = 0$.

It can be seen that there is room for a degree of arbitrariness between c and $V(\xi)$. Note that c is not a universal constant, but is effectively determined by the initial conditions. It is required to allow the advection velocity to vary between different trials (as observed by Lister and Stone [13]) while $V(\xi)$ remains universal. To remove the ambiguity, a condition fixing $V(\xi)$ is required.[13]

As argued in previous sections (3.3 and 4.3), there is a matching condition on $H(\xi)$ which states that the time dependence must vanish as we tend

[13] This condition is an arbitrary choice, but is required by the presence of c. Without it, V is only determined up to a constant. As well as altering V, different choices will result in a translation in the ξ co-ordinate. The previous use of ζ as the similarity variable corresponds to the condition $H'(0) = 0$.

to infinity in similarity variables. In this case, we must have,

$$H(\xi) \sim s_{\pm}|\xi| \quad \text{as} \quad \xi \to \pm\infty\,. \tag{54}$$

The constants, $s_{\pm}$, are identified as the tangents of the two cone angles.

The similarity solution is substituted into the governing equations. These are the integral representation (47), and the kinematic boundary condition ($\partial_t h + v\partial_z h = u$). Since the co-ordinates translate with the added velocity component, the latter disappears completely from the kinematic condition. In similarity variables it becomes,

$$-H + \frac{dH}{d\xi}\,(V + \xi) = U\,. \tag{55}$$

In the integral representation, the added velocity components do not in general cancel out. However, for a local similarity solution they must be made to. By considering asymptotic contributions to the integral from the intermediate conical region, Cohen *et al.* [5] derive the criterion:[14]

$$b = -\frac{1}{4}\left(\frac{s_+}{1+s_+^2} - \frac{s_-}{1+s_-^2}\right)\,, \tag{56}$$

This ensures that the logarithmic contributions cancel. The remaining constant c is, in principle, determined by applying the condition on V to the integral equation.

Cohen *et al.* [5] report solving this system numerically. They discretised $H(\xi)$ on a finite interval, $|\xi| \le \xi_\infty$. Assuming a linear approximation outside this interval, the logarithm in the boundary integral could be subtracted off explicitly. Using a simulation to provide a suitable initial configuration, Newton's method gave convergence to a solution. The solution is in good agreement with experiments reported in the same paper, as well as previous simulations by Lister and Stone [13]. Key parameters are given in the following table.

s_-	s_+	α_-	α_+	$H_{\min}$
0.105	4.81	6.0°	78.3°	0.0335

[14] This is effectively the same calculation as done by Lister and Stone [13], and yields the same expression for the log coefficient in terms of the cone angles.

5.5 Simulations and Experiments for General λ

So far, we have restricted attention to the special case of $\lambda = 1$. Zhang and Lister [26] performed some simulations for other λ, comparing their their results with experimental data from Cohen *et al.* [5]. More extensive experiments have recently been reported by Cohen and Nagel [4].

Since simulations for $\lambda \neq 1$ are computationally much more expensive, Zhang and Lister did not simulate entire drops, but concentrated on the pinching region. In their simplified scheme, only the central pinching region is evolved accurately. Outside this, conical approximations to the interface are used. These are eventually closed off with spherical caps to form a closed surface (required for the boundary integral). At each step, the central region is updated and then new cones are spheres are attached so as to ensure that the interface remains continuous and smooth. Typically, the cones were attached at a radius of about 10^3, and the spherical caps at about 10^4, in similarity variables.

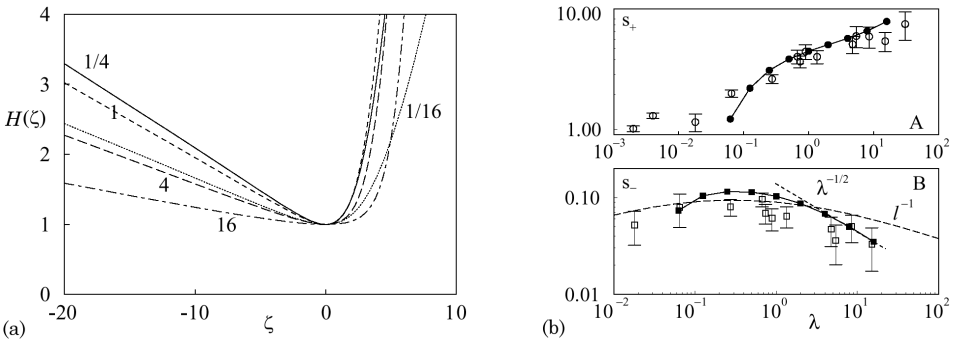

Figure 12: (a) *Self-similar profiles from the simulations of Zhang and Lister [26]. Lengths have been scaled by* $h_{\min}$*, and the minimum radius fixed at* $\zeta = 0$. (b) *Graphs of the variation of the cone slopes,* $s_\pm$*, with* λ*. The solid markers are the results of simulations [26], and the open markers are experimental measurements [5].*

Various simulations were performed for $\frac{1}{16} \leq \lambda \leq 16$. For $\lambda < \frac{1}{16}$, errors associated with the degenerate $\lambda = 0$ eigenmode were significant, and for $\lambda > 16$, the thread profile became oscillatory. For the successful simulations, asymmetric self-similar profiles were again found with $h \sim z \sim \tau$. Some of these are shown in figure 12a. As in the $\lambda = 1$ case, the whole pinching region is advected by an asymptotically large background velocity.

Whilst these solutions obey the asymptotic scaling with τ, they do not appear to follow the anticipated λ dependence. From the scaling arguments in section 5.1 one would expect $s_\pm \sim \lambda^{-1/2}$ at least for $\lambda \geq O(1)$. Whilst s_- does appear to satisfy this, s_+ certainly does not. As figure 12b shows, s_+ increases monotonically with λ, while s_- has a maximum near $\lambda = \frac{1}{4}$.

The experiments reported by Cohen and Nagel [4] and Cohen *et al.* [5] are in good agreement with the simulations of Zhang and Lister. Close to pinch-off, self-similar profiles are observed, which rapidly become conical away from the minimum radius. As predicted, the cone angles are are found to be independent of the faucet diameter, surface tension, and the density difference. There is also good agreement with the λ dependence found in the simulations, except for $\lambda \ll 1$.

There is now an interesting problem to account for the observed λ dependence of the cone angles, which is at odds with the simple scaling analysis. Despite useful contributions from Zhang and Lister [26] and Cohen and Nagel [4], a full explanation is still lacking. The discrepancy between the experiments and simulations for $\lambda \ll 1$ is also somewhat puzzling.

5.6 Post-Pinching Flow

To date, there has been no investigation into possible post-pinching flows in this regime. Unlike the other regimes discussed in this essay, we now have an exterior fluid to worry about. This allows interactions between the two receding tips, with the result that it may not be possible to treat them independently. Indeed, with the long-range character of the Stokes interaction, and in view of the contributions from the intermediate conical region, it seems unlikely that such a treatment would be possible.

For post-pinching flow, simulations are no longer as effective for finding a similarity solution (see section 6). However, it is certainly possible to start a simulation from a pair of perfect cones with a flow-profile given by the pre-pinching limit. Such a simulation is unlikely to converge so nicely to a similarity solution, but may well provide some useful insight into possible post-pinching behaviour.

With this, and perhaps some experimental evidence, an obvious similarity form might come to light. At least for $\lambda = 1$, one could then use the method of Cohen *et al.* [5] (see section 5.4) to find a full similarity solution.

6 Conclusions

Whilst significant progress has been made in analysing the flows just before pinch-off, less has been achieved for the corresponding post-pinching case. Leading up to pinch-off, a simulation can evolve a flow towards the singularity, perhaps converging to universal self-similar behaviour. A similarity shape can be inferred directly from the simulation results, or they can be used to provide guidance for proposing an appropriate form. For the post-pinching case, the simulation method is no longer as effective, since the initial conditions need to be applied at the singularity itself.

In the three regimes studied in this essay, the progress in terms of bridging the gap is very limited. The only fully explored case is the Navier–Stokes regime. This is also the most pleasing mathematically, since the system can be reduced to a set of ordinary differential equations which are readily solved by numerical methods [9]. However, it would appear that stochastic effects dominate close to pinch-off, as external noise triggers Rayleigh-like instabilities [21]. I find it unlikely that much further progress can be made here.

It is perhaps fortuitous that the other regimes do not appear to suffer from these instabilities. By analogy with the Rayleigh instability (which requires a wavelength greater than the circumference), this is most likely to be explained by their $O(1)$ aspect ratio close to pinch-off.

In the single fluid inviscid regime, we have a pre-pinching similarity solution [6], though this lacks solid experimental confirmation. In particular, it will prove difficult to verify the predicted angle in the dimple, since it is hidden by the rest of the drop. Work has been done on planar post-pinching flows [11], which now needs to be repeated in an axisymmetric geometry.

For two fluid pinch-off in the Stokes regime, experiments [4] and simulations [26] are in good agreement, suggesting self-similar pre-pinching solutions. Such a solution has been calculated explicitly [5] for a viscosity ratio, λ, equal to unity. When $\lambda \neq 1$ the problem is harder since there is a computationally expensive integral equation to solve. An investigation into the asymptotic form of post-pinching flows has yet to be carried out, but is likely to be complicated by interactions between the two receding tips.

For the cases I have studied, the pre-pinching flows are largely understood, while the post-pinching flows require more work. It would appear that the principle difficulties lie not so much in building the bridge, but more in trying to find some suitable ground on the other side.

References

[1] M.P. Benner, J.R. Lister, and H.A. Stone, *Pinching threads, singularities, and the number 0.0304...*, Phys. Fluids **8** (1996), 2827.

[2] M.P. Brenner, J. Eggers, K. Joseph, S.R. Nagel, and X.D. Shi, *Breakdown of scaling in droplet fission at high reynolds number*, Phys. Fluids **9** (1997), 1573.

[3] M.P. Brenner, X.D. Shi, and S.R. Nagel, *Iterated instabilities during droplet fission*, Phys. Rev. Lett. **73** (1994), 3391.

[4] I. Cohen and S.R. Nagel, *Testing for scaling behaviour dependence on geometrical and fluid parameters in the two fluid drop snap-off problem*, Phys. Fluids **13** (2001), 3533.

[5] I. Cohn, M.P. Brenner, J. Eggers, and S.R. Nagel, *Two fluid snap-off problem: Experiments and theory*, Phys. Rev. Lett. **83** (1999), 1147.

[6] R.F. Day, E.J. Hinch, and J.R. Lister, *Self-similar capillary pinchoff of an inviscid fluid*, Phys. Rev. Lett. **80** (1998), 704.

[7] H. Edgerton, G. Kayafas, and E. Jussim, *Stopping time: The photographs of Harold Edgerton*, Harry Abrams, New York, 1987.

[8] J. Eggers, *Universal pinching of 3D axisymmetric free-surface flow*, Phys. Rev. Lett. **71** (1993), 3458.

[9] ———, *Theory of drop formation*, Phys. Fluids **7** (1995), 941.

[10] ———, *Nonlinear dynamics and breakup of free-surface flows*, Rev. Mod. Phys. **69** (1997), 865.

[11] J. Keller and M.J. Miksis, *Surface tension driven flows*, SIAM J. Appl. Math. **43** (1983), 286.

[12] T.A. Kowalewski, *On the separation of droplets from a liquid jet*, Fluid Dyn. Res. **17** (1996), 121.

[13] J.R. Lister and H.A. Stone, *Capillary breakup of a viscous thread surrounded by another viscous fluid*, Phys. Fluids **10** (1998), 2758.

[14] D.T. Papageorgiou, *Analytical description of the breakup of liquid jets*, J. Fluid Mech. **301** (1995), 109.

[15] ———, *On the breakup of viscous liquid threads*, Phys. Fluids **7** (1995), 1529.

[16] D.H. Peregrine, G. Shoker, and A. Symon, *The bifurcation of liquid bridges*, J. Fluid Mech. **212** (1990), 25.

[17] J.A.F. Plateau, *Statique expérimentale et thorique des liquides soumis aux seules forces moléculaires*, Gauthier-Villars, Paris, 1873.

[18] J.M. Rallison and A. Acrivos, *A numerical study of the deformation and burst of a viscous drop in an extensional flow*, J. Fluid Mech. **89** (1978), 191.

[19] Lord Rayleigh, *On the stability of liquid jets*, Proc. London Math. Soc. **10** (1878), 4.

[20] ———, *On the stability of a cylinder of viscous fluid under a capillary force*, Phil. Mag. **34** (1892), 145.

[21] X.D. Shi, M.P. Brenner, and S.R. Nagel, *A cascade of structure in a drop falling from a faucet*, Science **265** (1994), 219.

[22] G.I. Taylor, *The fomation of emulsions in definable fields of flow*, Proc. Royal. Soc. London (A) **146** (1934), 501.

[23] L. Ting and J.B. Keller, *Slender jets and thin sheets with surface tension*, SIAM J. Appl. Math. **50** (1990), 1533.

[24] M. Tjahjadi, H.A. Stone, and J.M. Ottino, *Satellite and subsatellite formation in capillary breakup*, J. Fluid Mech. **243** (1992), 297.

[25] S. Tomotika, *On the instability of a cylindrical thread of a viscous liquid surrounded by another viscous liquid*, Proc. Royal. Soc. London (A) **150** (1935), 322.

[26] W.W. Zhang and J.R. Lister, *Similarity solutions for capillary pinch-off in fluids of differing viscosity*, Phys. Rev. Lett. **83** (1999), 1151.